Circular Die Swell Evaluation of LDPE Using Simplified Viscoelastic Model

Limtrakarn W.

Department of Mechanical Engineering, Faculty of Engineering, Thammasat University, Pathumthani, Thailand
E-mail address: limwiroj@engr.tu.ac.th

Pratumwal Y., Krunate J., Prahsarn C., Phompan W., Sooksomsong T., Klinsukhon W.

National Metal and Materials Technology (MTEC), Pathumthani, Thailand

Abstract

Simplified viscoelastic model based finite element method was presented to evaluate circular die swell of LDPE. Differential viscoelastic models were firstly described for the incompressible viscoelastic flow with isothermal extrusion, and simplified viscoelastic model (SVM) was then selected for viscoelstic component in extra stress terms. Discrete elastic viscous stress splitting (DEVSS) method was used to stabilize elliptic term in momentum equations. Mini–element method for hexahedral element was applied to stabilize equal order velocity pressure interpolation. Interface–tracking approach was used to detect the position and moving of the free surface at extrudate region. In experiment, circular die was selected to study LDPE extrusion flow. The measured viscoelastic properties were employed as input data in LDPE flow simulation. CCD camera was used to capture extrudate swell. Simplified viscoelstic model was then used to predict extrudate swell in three flow rate conditions, 100, 264, and 490 mm^3/s. Compared with experimental results, the die swell predicted by SVM were 1.37%, 2.37%, and 5.5% different, for the three flow rate conditions, respectively. The results showed that simplified viscoelastic model could be employed to predict circular die swell.

Keywords*: Die swell, Simplified viscoelastic model, LDPE*

1 Introduction

Die swell is a common behavior observed in the polymer extrusion process. Accurate prediction of an extrudate dimension is important to die design and product quality. Extrusion is used to produce fibers, films, tubing, and a variety of profiles. Extrusion process is a very complex task and requires detailed knowledge of material characteristics, flow phenomena, and extrusion processing experience [1]. The appropriate design of an extrusion die and its process parameters are extremely important to achieve the desired shape and accurate dimensions of the extruded product. Die design for a new product and cost reduction is developed on the basis of previous experience and experimentation. Trials and errors as well as experiment tasks have been the common practice to design the properly extrusion die with expensive cost and time. The proper design of extrusion dies can be facilitated by computational fluid dynamics (CFD) analysis. Costly experiments and in-plant trials can be reduced by CFD simulation. Extrusion die is design by several polymer flow simulation software such as Ansys/Polyflow, OpenFoam, Flow2000, Dieflow, HyperXtrude, etc. [2] CFD simulation has great potential to predict important interior details of the extrusion process such as velocity, shear stress, pressure, and temperature fields in the region of interest, which is not possible to do experimentally.

In extrusion processes, the swelling of the extrudate is controlled by a physical mechanism: relaxation of the polymeric liquids originating from the recoiling and relaxing of the stretched polymer chains as they exit from the die. In order to accurately simulate polymer extrusion processes, the computational model must account for this mechanism and capture the effect of non–linear polymer or viscoelasticity. Non–linear viscoelastic models have been developed, including the Kay–Bersteinighly branched polymKearsly–Zappa

(KBKZ) integral model and the exponent Phan–Thien–Tanner (EPTT) differential model. These two models give good predictions of the behavior of polymeric fluids under rheometric and extrusion flows [3–7]. The die swell of low density polyethylene (LDPE) melt was simulated [6] in a long die using four types of damping functions of the KBKZ model to examine the cause of the exaggerated swelling ratios. The pom–pom model is a molecular constitutive model for modeling the flow behavior of polymeric fluids such as the LDPE. The double convected pom–pom (DCPP) model [8] was proposed to predict the behavior of polymeric fluids under rheometric and complex flows. The results were in good agreement with the experimental data [9]. Simplified viscoelastic model (SVM) [10] was presented and included the effect of the first normal stress difference to account for one of the key contributions of polymer viscoelasticity to the die–swell of polymeric melts. Computationally, it is very cost–effective in comparison with the other non–linear viscoelastic models [11], and gives reasonably good predictions of complex viscoelastic fluid flows. In the present work, prediction of the SVM on the die swell of a well–characterized commercial LDPE through a long die had been described and shown to be in good agreement with the result of the other advanced constitutive models.

2 Theoretical formulation

The equations for the incompressible viscoelastic flow with isothermal extrusion are represented by the conservation of mass and momentum, as well as a constitutive equation.

2.1 *Conservation equations*

The equations of conservation of mass and momentum can be expressed as

$$\nabla \cdot \mathbf{V} = 0 \tag{1}$$

and

$$\rho \frac{D\mathbf{V}}{Dt} = -\nabla p + \nabla \cdot \boldsymbol{\sigma} \tag{2}$$

where ρ is the density, $\mathbf{V}$ is the velocity, p is the pressure, t is time, and $\boldsymbol{\sigma}$ is the stress tensor and is given by a constitutive equation.

2.2 *Constitutive equations*

Elastic viscous split stress method is applied to decompose the stress tensor in 2 components: pure viscous stress ($\boldsymbol{\sigma}_s$) and viscoelastic stress ($\boldsymbol{\sigma}_v$).

$$\boldsymbol{\sigma} = \boldsymbol{\sigma}_s + \boldsymbol{\sigma}_v \tag{3}$$

The pure viscous stress is represented for generalized Newtonian fluids and given as

$$\boldsymbol{\sigma}_s = 2\eta\mathbf{D} \tag{4}$$

where η is shear viscosity coefficient and can be expressed by the Carreau Yasuda model as following,

$$\eta = \eta_\infty + (\eta_0 - \eta_\infty)(1+(\lambda \dot{\gamma})^a)^{(n-1)/a} \tag{5}$$

where η_0 and η_∞ are the shear viscosities at the limits of zero and infinite shear rate, respectively, λ is the relaxation time, n describes the slope of the power-law region, and $\dot{\gamma}$ is the local shear rate.

$$\mathbf{D} \text{ is the rate of deformation tensor} = \frac{\nabla V + (\nabla V)^T}{2} \tag{6}$$

where $\nabla\mathbf{V}$ and $(\nabla\mathbf{V})^T$ are the velocity gradient and transpose of the velocity gradient.

In this paper, the viscoelastic components were described in the Simplified Viscoelastic model (SVM). The SVM or light viscoelastic model is an extension of the generalized Newtonian fluid models and accounts for viscoelastic effects in a simple form. The viscoelastic stress tensor for the SVM is given as

$$\boldsymbol{\sigma}_v = \begin{bmatrix} \sigma_{xx} & \tau_{xy} & 0 \\ \tau_{yx} & 0 & 0 \\ 0 & 0 & 0 \end{bmatrix} = \begin{bmatrix} \psi\mu(\dot{\chi})\dot{\chi} & \eta(\dot{\gamma})\dot{\gamma} & 0 \\ \eta(\dot{\gamma})\dot{\gamma} & 0 & 0 \\ 0 & 0 & 0 \end{bmatrix} \tag{7}$$

The shear stress is related to the shear rate dependence of shear viscosity $\eta(\dot{\gamma})$ and defined in the usual way of the generalized Newtonian fluid models. The first normal stress σ_{xx} is given by $\psi\mu(\dot{\chi})\dot{\chi}$, which consist of a weighting factor ψ, a normal viscosity $\mu(\dot{\chi})$, and a viscoelastic variable $\dot{\chi}$. The normal viscosity $\mu(\dot{\chi})$ can be defined in the same way as the shear viscosity $\eta(\dot{\gamma})$ by replacing $\dot{\chi}$ with $\dot{\gamma}$. In this paper Bird – Carreau model is applied for μ.

$$\eta = \eta_\infty + (\eta_0 - \eta_\infty)(1+(\lambda\dot{\gamma})^2)^{(n-1)/2} \quad (8)$$

The viscoelastic variable $\dot{\chi}$ is governed by a transport equation with a shear rate dependent relaxation time λ.

$$\lambda(\dot{\chi})\frac{D\dot{\chi}}{Dt} + \dot{\chi} = \dot{\gamma} \quad (9)$$

Equation (9) is based on the idea of a memory effect from viscoelastic fluids. The weighting factor ψ controls the swelling intensity against flow rate and the relaxation time controls the development of the extrudate diameter along the jet.

3 Experimental methods

A commercial LDPE (PETLIN LD C150Y) supplied by PETLIN (Malaysia) SDN BHD, was used in this study. Its melt flow rate is 5 dg/min (ISO 1133). Some specifications of the resin are as follows: density = 0.921 g/cm^3 (ISO 1183A), tensile strength at yield = 15 MPa (ISO R527-3), and ultimate elongation = 610% (ISO R527-3).

3.1 *Linear Rheology*

Storage modulus G'(ω) and loss modulus G"(ω) were obtained from small amplitude oscillatory shear experiments, performed using a 25mm parallel plate geometry on Gemini 200HR Nano rotational rheometer. Data was obtained at 180°C. The equilibration time was set to 5 minutes in order to maintain thermal equilibration before data acquisition began.

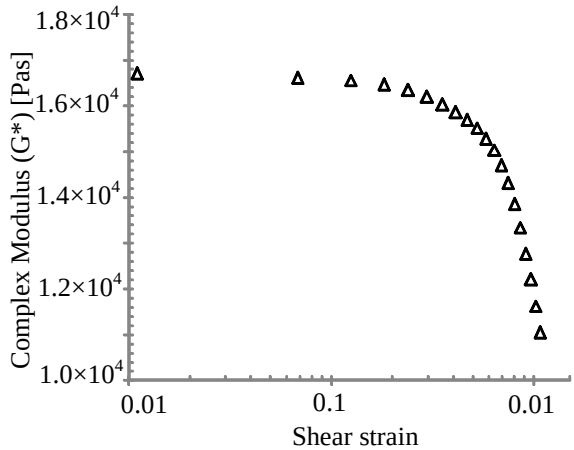

Figure 1: Complex modulus (G*) data of the LDPE sample obtained from the stress sweep test at 180°C.

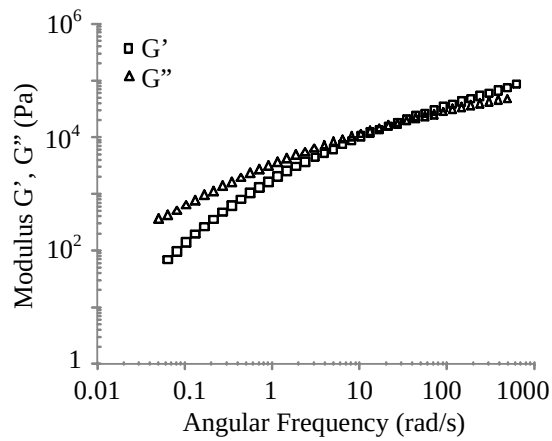

Figure 2: The experimental G' and G" data of the LDPE sample obtained from the dynamic frequency sweep with strain equal to 5% (0.05) at 180°C.

3.2 *Nonlinear Rheology*

Steady shear and step shear experiments were performed using Gemini 200HR Nano rotational rheometer of Malvem-Bohlin Instruments. Steady shear experiments were performed at 180°C using parallel plate geometry (25 mm diameter, gap 1 mm) by ramping the shear rate from 0.0001 to 1000 s^{-1}. The first normal stress difference was also obtained from normal force measurements. Step shear experiments were performed using 25 mm. parallel plate geometry at 180°C. For higher shear rates (> 3 s−1), the transient viscosity data was not reliable since the specimen was forced out from the gap between the parallel plates.

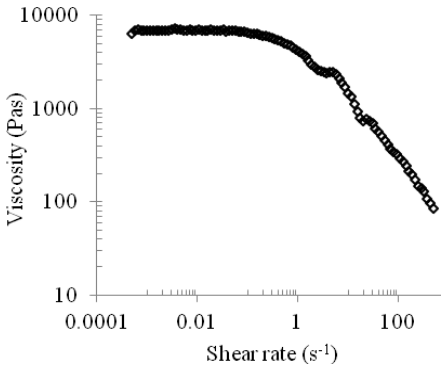

Figure 3: The steady shear viscosity data of the LDPE sample obtained from the steady rate sweep at the temperature of 180°C.

3.3 *Experimental setup*

The extrusion flow experiments were performed on a twin-screw extruder (Labtech Engineering, LTE-20-32). In this work, the effects of test volumetric flow rate on the extrudate swell of LDPE were considered for the test temperature range of 160-180°C. The screw speed (rpm) / feeder speed (rpm) were set to be 25/5, 70/7 and 120/10 to obtain volumetric flow rate 100, 264, and 490 mm^3/s, respectively.

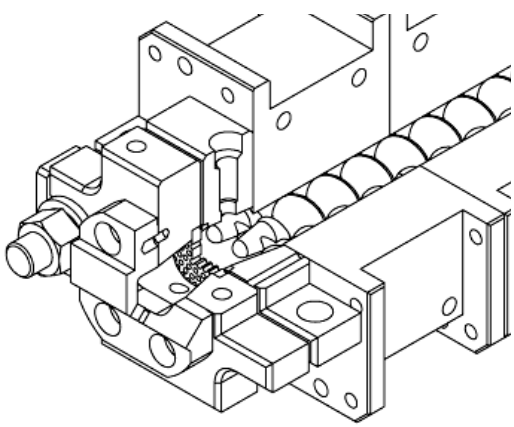

Figure 4: Twin screw machine.

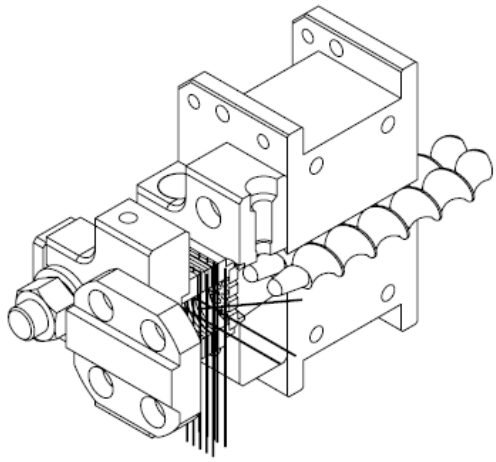

Figure 5: Temperature sensor.

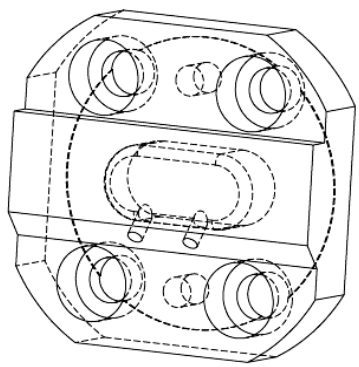

Figure 6: Circular Die.

3.4 *Extrudate swell measurement*

The extudate swell diameters of the polymer melts were directly measured by determining the size of the extrudate diameter in the fully swollen (2 in. away from the die exit) [12]. The pictures were taken from high speed camera (Nikon D90) couple with TAMRON SP AF 90mm macro. The experiments were repeated for three times to assure the obtained results.

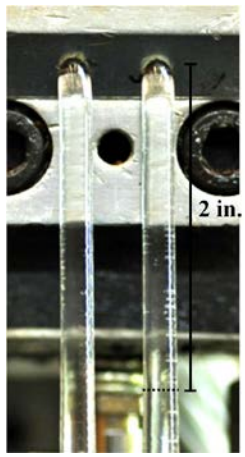

Figure 7: Extrudate swell of LDPE, test temperature range 160-180°C and Screw speed/ feeder speed25/5 (volumetric flow rate 99.96 mm^3/s).

4 Computational model and technique

A finite element method based on discrete elastic viscous stress splitting (DEVSS) and a streamline upwinding (SU) scheme, was used to solve the governing equations. The DEVSS scheme can be readily applied to all the viscoelastic constitutive equations [10] as the constitutive equation need not be rewritten. The implementation of the DEVSS/SU scheme permits the use of a lower order interpolation scheme for the viscoelastic unknown variables without generating an ill-posed problem. This can significantly save computational costs. For the SVM and Bird – Carreau model, Picard iteration is used to solve the governing equations with a AMF direct solver as it gives a better convergence for a fluid with the power-law index < 0.7.

For the numerical results presented below, the Weissenberg (Wi) number is defined as

$$Wi = \dot{\gamma}\lambda_m \tag{10}$$

where λ_m is the mean relaxation time and $\dot{\gamma}$ is the nominal shear rate and is defined as

$$\dot{\gamma} = \frac{U_m}{r} = \frac{Q}{Ar} = \frac{4Q}{\pi r^3} \tag{11}$$

where Q is the flow rate, U_m is the mean velocity, A is the cross sectional area and r is the radius of the die. For a multimode spectrum, the λ_m can be estimated from [9]

$$\lambda_m = \frac{\sum_{i=1}^{M} \lambda_i^2 G_i}{\sum_{i=1}^{M} \lambda_i G_i} \tag{12}$$

where i represents the i^{th} relaxation mode, M is the total number of different modes, λ_i (s) is the i^{th} linear relaxation time and G_i (Pa) is the i^{th} plateau modulus.

4.1 *DEVSS method [13]*

To restrain and even eliminate the instability from the loss of characteristics of the governing equations in symbolizing elliptic behavior, the elastic viscous stress splitting (EVSS) method was proposed by Perera and Walters [14] to retain an elliptic term and consequently the viscous contribution in the momentum equation. But to achieve this end the constitutive equation has to be modified. Moreover, the convected derivative of the rate of strain tensor emerges, which requires calculation of a second-order derivative of the velocity field. So, it is difficult to apply this approach to complex constitutive equations.

The DEVSS method is proposed as a discrete version of the elastic viscous stress splitting method. In this method a stabilizing elliptic term is introduced into the discretized momentum equation in the absence of a purely viscous contribution or as the viscous contribution is negligible in comparison with the viscoelastic contribution and can be numerically implemented in a convenient manner. To construct the DEVSS method, an auxiliary variable $\underline{D}$ as a discrete counterpart of the rate of deformation tensor and an independent variable is introduced and determined in terms of satisfaction of

$$\underline{D} - D = 0 \tag{13}$$

in a weighted average form, i.e. $(\boldsymbol{W}, \underline{D} - D) = 0$, with $\boldsymbol{W}$ denoting a suitable weighting function. Further, taking the divergence of Eq. (13) and adding $-2\,\eta_e\,\nabla\cdot(\underline{D} - D)$ into the momentum conservation equation with the use of Eq. (2) result in

$$\rho\frac{D\mathbf{V}}{Dt} = -\nabla p + \nabla\cdot\boldsymbol{\tau} - 2\,\eta_e\,\nabla\cdot(\underline{D} - D) \qquad (14)$$

4.2 *Free surface condition*

Interface – tracking approach is used to detect the position and moving of the free surface at extrudate region. The kinematic conditions are approached for moving interface. The large deformation appears on free surface interface. The evolution is implemented to obtain solution convergence.

The following three boundary conditions are defined on a free surface.

$$v_r\,n_r + v_z\,n_z = 0 \qquad (15)$$

$$t_r\,n_r + t_z\,n_z = S\left(\frac{1}{\rho_1}+\frac{1}{\rho_2}\right) = 0 \qquad (16)$$

$$t_r\,n_r - t_z\,n_z = 0 \qquad (17)$$

with variables specification of radial velocity (v_r), axial velocity (v_z), components of the unit normal to the free surface (n_r, n_z), surface force normal to the surface (t_r, t_z), principal radii of curvature (r_1, r_2) and surface tension coefficient (S). When S equals zero, it represents free slip condition. While S equal one, it is equivalent to a no–slip boundary condition. An evolution method (typical iterative approach) for modeling a free surface flow involves enforcing the boundary conditions of equations (16) and (17).

In order to avoid over distortion of elements, a remeshing technique is used to propagate the motion of the free surface into the mesh. The mesh is considered as a deforming elastic grid. A remeshing based on the minimization of the deformation energy of a grid is proposed. An elastic response corresponds to the angular deformation of the corners, of the diagonal of elements, and of the side of elements. Energy may be associated with the deformation of the grid, and the remeshing is the result of the minimization of that energy: one solves an elastic problem.

4.3 *Geometry and boundary conditions*

The computational geometry consists of a quarter of a cylinder with the dimensionless length $z^* = 40$ and the radius $r_1^* = r_2^* = 1$. Figure 5 shows the geometry used in the simulation and the computational mesh with the boundary conditions. Fully developed velocity and stress profiles are specified at the inlet BD1. A vanishing force condition is implemented at the exit BD2. Care is taken to ensure that the extrudate is long enough to satisfy this condition at BD2. A no slip condition is applied at the wall of die BD3. BD4 is the free surface, which is a priori unknown. Surface tension is neglected; hence a vanishing force condition is applied at BD4. Next to this, the kinematic condition, $\mathbf{v}\cdot\mathbf{n} = 0$ is solved, where $\mathbf{n}$ is the normal vector to the free surface. This implies that there is no flow through the free surface. For BD5 and BD6, a symmetry condition is specified by imposing zero values for the normal velocity and the tangential force.

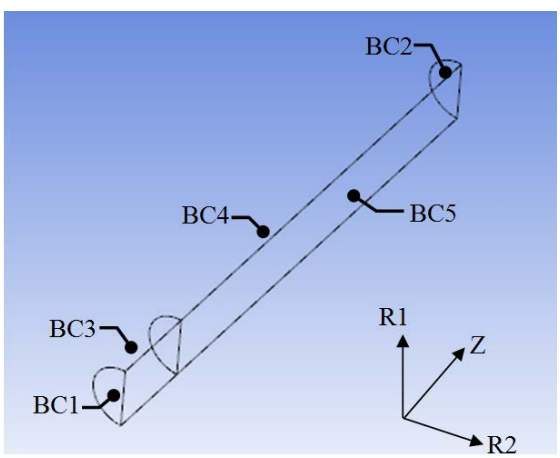

Figure 8: 3–D extrusion flow geometry in a quarter of a cylinder with origin at $r_1 = 0$, $r_2 = 0$ and $z = 0$ with different boundaries.

5 Results and discussion

Finite element model with 21,952 nodes and 19,206 elements was generated to simulate extrudate. This is necessary for simulations involving the discretization of non-linear viscoelastic models using the combined DEVSS/SU scheme [9]. The detail of mesh was given in Figure 9. The velocity field obtained from SVM was shown in Figures 10a. The dimensionless pressure distribution is given as $P^* = P/p_a$, where P is the pressure difference along the flow direction and p_a is the atmospheric pressure. The dimensionless velocity is $v^* = v/U_m$, where U_m is the mean velocity of the flow. With increasing Weissenberg (Wi), the shear-thinning velocity profile is more pronounced. The swelling ratio, S_W could be measured with respect to either r_1 or r_2 and the same results are obtained from the two directions in the present work.

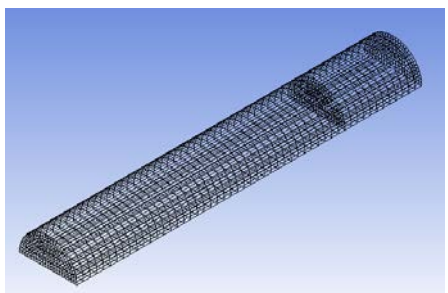

(a) Mesh 1 (M1)

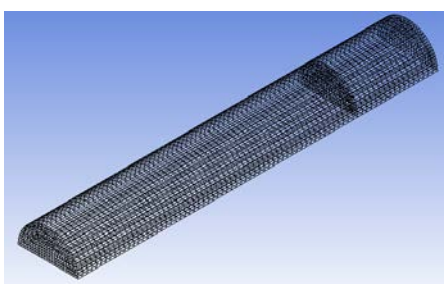

(b) Mesh 2 (M2)

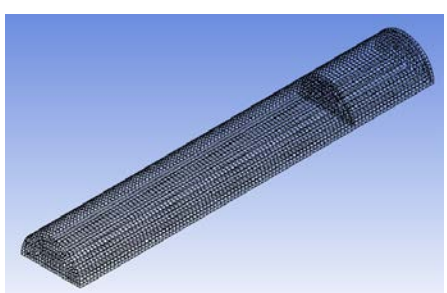

(c) Mesh 3 (M3)

Figure 9: Mesh for simulation of extrusion flow.

The swelling ratios obtained from finite element model were found in good agreement with experimental results. The largest difference of the S_W in the range of Wi used was 2%. Similar results were obtained using the SVM in the same range of Wi.

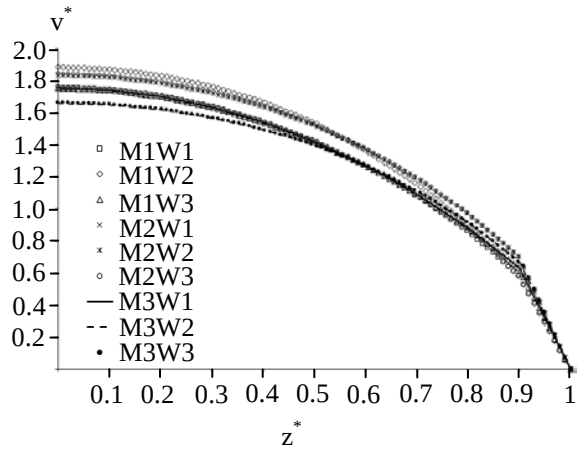

(a) Velocity profile across the r_2–axis (r_2–axis, $r_1^* = 0$ and $z^* = 4$)

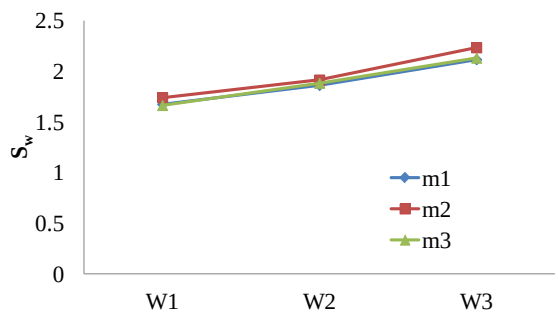

(b) Plot of S_W against Wi

Figure 10: The simulation results obtained from finite element model using SVM: (a) velocity profile across the r_2–axis (r_2–axis, $r_1^* = 0$ and $z^* = 4$) and (b) a plot of S_W against Wi.

5.1 *Extrudate swell in viscoelastic fluids*

Simulations were carried out for viscoelastic models. This is to validate the accuracy of the predictive power of SVM in modeling the die-swell behavior of LDPE fluid in extrusion flow, through comparison with Wi from W_1, W_2, and W_3. Figure 11 showed the contour plots of the shear rate for the three flow conditions. The plots of the pressure distribution along the flow direction at W_1, W_2, W_3 (Figures 12a–c) showed that there were also in good agreements amongst the three models.

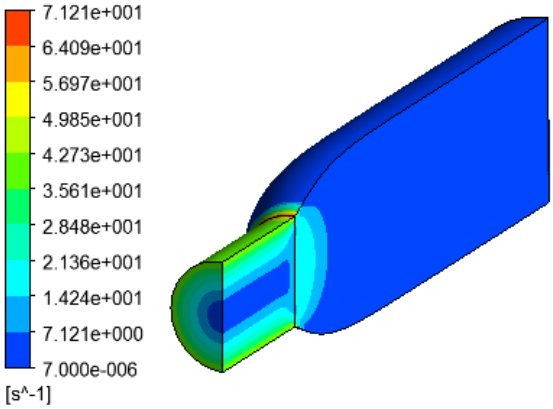

a) Flow rate 100 mm^3/s

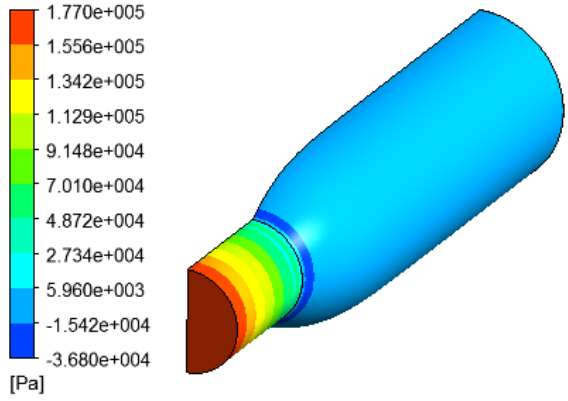

(a) A plot of pressure distribution along the flow direction (z-axis, $r_1^* = 0$ and $r_2^* = 0$) at W1.

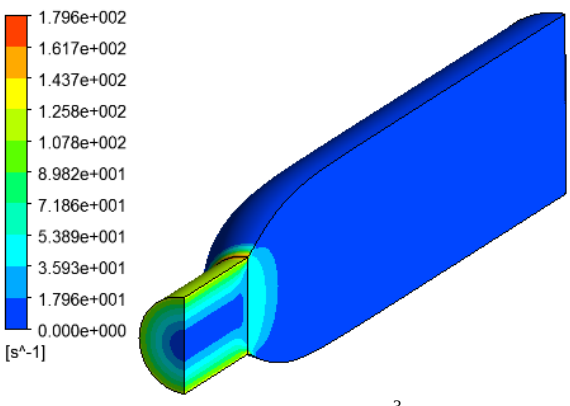

(b) Flow rate 264 mm^3/s

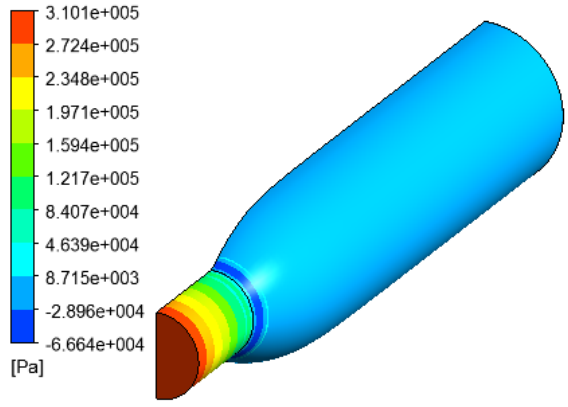

(b) Contour plots of pressure distribution along the flow direction at W2.

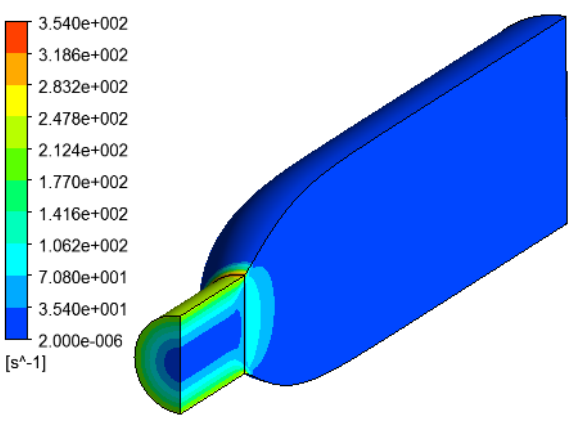

(c) Flow rate 490 mm^3/s

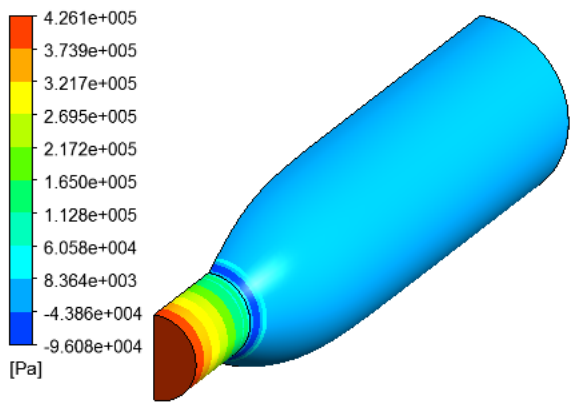

(c) Contour plots of pressure distribution along the flow direction at W3.

Figure 11: The Contour profile images obtained by using SVM at different flow rates (a) 100 mm^3/s; (b) 264 mm^3/s and (c) 490 mm^3/s.

Figure 12: The simulation results obtained from three flow rate conditions: (a), (b), and (c) a plot of pressure distribution along the flow direction (z-axis, $r_1^* = 0$ and $r_2^* = 0$) at W1, W2, and W3, respectively.

Also in Figure 12, the plot of the S_W against Wi for the three conditions showed that there are reasonable agreements in the prediction of the extrudate swelling ratio. Taking the experiments as a reference, the percentage relative difference in the prediction of the S_W obtained from SVM at W_1, W_2, and W_3 were 1.525%, 0.354%, and 8.017%, respectively. Although SVM is not a full viscoelastic constitutive model, it still could give a good prediction on the die-swell ratio of polymer extrusion flow from along straight die. This was not so surprising because the viscoelastic effects were predominately from the contributions of the non-linear shear viscosity and pressure difference in these particular types of extrusion flows.

6 Conclusions

Computer simulations of the extrusion flow process had been carried out, using both viscoelastic and non-Newtonian models. Through comparisons of viscoelastic model and experiments, the accuracy of the SVM in predicting the die-swell behavior of polymeric fluid in extrusion flow had been verified and was found in reasonably good agreement with experimental results. The effects of viscoelasticity of a polymer melt in extrusion processes had also been quantified. A surprising cooperative effect of the viscoelasticity had been identified. Although the SVM captures some essential physics of polymer extrusion processes, it should be noted that it does not account for the full viscoelastic effect of a polymeric fluid, such as the second normal stress difference and extensional viscosity, which seem to have no significant effects on the particular flow studied here.

Acknowledgments

The authors are pleased to acknowledge the Thailand Commission on Higher Education of Thailand (the National Research University Project), the National Science and Technology (NRCT), the Thailand Research Fund (TRF), Royal Project Foundation, Thammasat University, and the National Metal and Materials Technology Center (MTEC) for supporting this research work.

References

[1] Kostic, M. M., Reifschneider, L. G., 2006, *Design of Extrusion Dies*, Encyclopedia of Chemical Processing, 633-649.

[2] Pepliński, K., Mozer, A., 2011**,** Design of Extrusion Die for Plastic Profile using ANSYS/Polyflow software, *Journal of Polish CIMAC*, 6(3): 221–226.

[3] Luo, X-L., Tanner, R.I., 1986a. A streamline element scheme for solving viscoelastic flow problems, part I: differential constitutive models., *Non-Newtonian Fluid Mechanics*, 21: 179–199.

[4] Luo, X-L., Tanner, R.I., 1986b. A streamline element scheme for solving viscoelastic flow problems, part II: integral constitutive models., *Non-Newtonian Fluid Mechanics*, 22: 61–89.

[5] Goublomme, A., Draily, B., Crotchet, M.J., 1992. Numerical prediction of extrudate swell of a high density polyethylene., *Non-Newtonian Fluid Mechanics*, 44: 171–195.

[6] Huang, S.X., Lu, C.J., 2006. Stress relaxation characterisitics and extrudate swell of the IUPAC-LDPE Melt., *Non-Newtonian Fluid Mechanics*, 136: 147–156.

[7] Mitsoulis, E., 2007. Past and new developments in the numerical simulation of polymer flows with the K-BKZ model. In: *ESAFORM Conference on Material Forming*.

[8] Clemeur, N., Rutgers, R.P.G., Debbaut, B., 2003. On the evaluation of some differential formulation for the pom–pom constitutive model., *Rheological Acta*, 42: 15.

[9] Clemeur, N., Rutgers, R.P.G., Debbaut, B., 2004. Numerical simulation of abrupt contraction flows using the double convected pom–pom model., *Journal of Non-Newtonian Fluid Mechanics*, 117 (2–3): 193–209.

[10] Fluent, 2008. Polyflow 3.12 User's Guide. F. Inc. 3.11, 664.

[11] Debbaut, B., Marchal, T., 2008. Numerical simulation of extrusion process and die design for industrial profile, using multimode pompom model. Plastics, *Rubber and Composites*, 37: 142–150.

[12] Brydson, J.A. 1981. *Flow Properties of Polymer Melts*, 2nd ed, London: Gorage Godwin.

[13] Han, X., Li, X., 2008. A mixed finite element scheme for viscoelastic flows with XPP model. *Acta Mech Sin*, 24: 671–680.

[14] M.G.N. Perera and K. Walters, 1977, Long-range memory effects in flows involving abrupt changes in geometry, Part I. Flows associated with L-shaped and T-shaped geometries, *J. Non-Newtonian Fluid Mech*, 2 (2): 49–81.

[15] Pichelin, E., Coupez, T. 1998. Finite element solution of the 3D mold filling problem for viscous incompressible fluid, Comput., *Methods Appl. Mech. Engrg*, 163: 359-371.

[16] Yu, H., C. Kietzmann, P. Cook, S. Xu, F. Costa, and P. K. Kennedy. 2004. A New Method for Simulation of Injection Molding, *SPE ANTEC Proceedings*, Chicago: 641-644.

[17] Liang, J.Z., Yang, J., Tang, C.Y., 2010. *Die-swell behavior of PP/Al(OH)3/Mg(OH)2 flame retardant composite melts*. Polymer testing, 1-5.

[18] Fulchiron, R., Revenu, P., Kim, B.S., Carrot, C., Guillet, J., 1997. Extrudate swell and isothermal melt spinning analysis of linear low density polyethylene using the Wagner constitutive equation, *J. Non-Newtonian Fluid Mech*., 69: 113-136.

[19] Guenette, R., Fortin, M., 1995. A new mixed finite element method for computing viscoelastic flows, *J. Non-Newtonian Fluid Mech*., 60: 27-52.

[20] Ganvir,V., Lele, A., Thaokar, R., Tautham, B.P., 2009. Prediction of extrudate swell in polymer melt extrusion using an Arbitrary Lagrangian Eulerian (ALE) based finite element method, *J. Non-Newtonian Fluid Mech*., 156: 21-28.

[21] Vaddiruju, S.R., 2005. M.D. Thesis, Northern illinois university, USA.